[redacted]

Copy No. 20

RM No. A9C07

NACA

RESEARCH MEMORANDUM

AERODYNAMIC STUDY OF A WING-FUSELAGE COMBINATION EMPLOYING A WING SWEPT BACK 63°. - INVESTIGATION AT A MACH NUMBER OF 1.53 TO DETERMINE THE EFFECTS OF CAMBERING AND TWISTING THE WING FOR UNIFORM LOAD AT A LIFT COEFFICIENT OF 0.25

By Robert T. Madden

Ames Aeronautical Laboratory
Moffett Field, Calif.

[redacted]

NATIONAL ADVISORY COMMITTEE FOR AERONAUTICS

WASHINGTON

May 6, 1949

[redacted]

NACA RM No. A9C07 [redacted]

NATIONAL ADVISORY COMMITTEE FOR AERONAUTICS

RESEARCH MEMORANDUM

AERODYNAMIC STUDY OF A WING-FUSELAGE COMBINATION EMPLOYING A WING SWEPT BACK 63°.- INVESTIGATION AT A MACH NUMBER OF 1.53 TO DETERMINE THE EFFECTS OF CAMBERING AND TWISTING THE WING FOR UNIFORM LOAD AT A LIFT COEFFICIENT OF 0.25

By Robert T. Madden

SUMMARY

Tests have been performed at a Mach number of 1.53 with a wing-fuselage combination having a wing with 63° leading-edge sweep, an aspect ratio of 3.46, and a taper ratio of 0.25. This wing had an NACA 64A005 thickness distribution parallel to the plane of symmetry and was cambered and twisted. The principal object of the investigation was to determine the effects of camber and twist on the maximum lift-drag ratio and pitching-moment characteristics. The results obtained from these tests are compared with those of a preceding investigation employing the same fuselage and wing plan form but with a wing having an NACA 64A006 thickness distribution and no camber or twist. Tests were also performed to determine the characteristics of configurations obtained by rotating the cambered, twisted wing panels to 67° and 70° leading-edge sweep. The effects of Reynolds number were also investigated.

At a Reynolds number of 0.84 million, the thinner, cambered, and twisted-wing configuration with 63° leading-edge sweep had a maximum lift-drag ratio of 8.3 as compared with 7.2 for the similar configuration of the earlier investigation. This increase resulted from a decrease in minimum drag coefficient, a displacement of the minimum of the drag curve to a positive lift coefficient and a decrease in the rate of drag rise with increased lift coefficient. Although the total center-of-lift travel was greater for the cambered-wing configuration, the change in center-of-lift location with lift coefficient near that for maximum lift-drag ratio was reduced.

As in the earlier investigation, the sweep angle for maximum lift-drag ratio at a Mach number of 1.53 was found to be approximately 67°. The magnitude of the maximum lift-drag ratio increased with

[redacted]

increased Reynolds number. Values of 7.3 and 8.3 were obtained at Reynolds numbers of 0.62 and 0.84 million, respectively, with the 63° wing configuration, and values of 6.6, 7.7, and 9.0 were obtained at Reynolds numbers of 0.31, 0.62, and 0.95 million, respectively, with the 67° configuration. These results indicate that further improvement may be expected at Reynolds numbers beyond the range of the small-scale tests.

INTRODUCTION

This report is the second on a series of tests which have been made at a Mach number of 1.53 to determine the lift, drag, and pitching-moment characteristics of wing-fuselage configurations using wings with large angles of sweepback. The original configuration, designed with the theoretical results of reference 1 as a guide, had a wing with 63° of leading-edge sweep, an aspect ratio of 3.42, a taper ratio of 0.25, and an NACA 64A006 section parallel to the plane of symmetry. The fuselage had a fineness ratio of 12.5. The experimental results obtained with this configuration at a Mach number of 1.53 are presented in reference 2, wherein the effects of Reynolds number and the effects of varying the sweep angle by rotating the wing panels about the midpoint of the root chord are also discussed. The aerodynamic characteristics of the original configuration (63° sweep) are also being studied at subsonic and lower supersonic speeds; the results obtained to date are presented in references 3 and 4.

The linear theory indicated that values of maximum lift-drag ratio greater than 10 to 1 could be maintained with this combination up to Mach numbers of approximately 1.5. The results of tests showed, however, that the maximum lift-drag ratio was less than predicted by theory. At low lift coefficients, the rate of drag increase with lift coefficient was greater than predicted by the inviscid theory, and furthermore, the static longitudinal stability was less than theory indicated. These discrepancies were attributed to boundary-layer separation. This separation was caused by the nature of the chordwise pressure gradients which theory indicates are highly adverse over the wing area near the leading edge when the wing is at moderate angles of attack. The adverse gradients are the greatest, and therefore the most detrimental, on the outboard sections because the induced upwash increases with distance from the root chord. These pressure gradients near the tip were so adverse that the boundary layer remained separated over the entire chord at relatively low angles of attack. The accompanying loss of lift and increase in drag were responsible for the discrepancies noted in reference 2.

It was considered probable that some improvement in the aerodynamic characteristics of this configuration would result if the nature of the pressure distribution due to angle of attack were modified to decrease the adverse pressure gradients. A possible means of decreasing the influence of the pressure distribution was shown in reference 1, where camber and twist were used to obtain a uniform lifting pressure distribution (neutral pressure gradients) at a specified lift coefficient and Mach number. Using this method, a cambered, twisted wing was designed which had the same wing plan form as the basic configuration of the preceding investigation. It is the purpose of the present report to describe the tests conducted with the modified wing at a Mach number of 1.53 to determine the effects of camber and twist on the maximum lift-drag ratio and pitching-moment characteristics. As in the previous investigation, the effects of variations in sweep and Reynolds number on these parameters were also studied.

SYMBOLS

Basic Symbols

A	aspect ratio $\left(\frac{b^2}{S}\right)$
b	wing span measured perpendicular to plane of symmetry, inches
c	wing chord measured parallel to plane of symmetry, inches
$\bar{c}$	mean aerodynamic chord $\left(\frac{\int_0^{b/2} c^2\, dY}{\int_0^{b/2} c\, dY}\right)$, inches
$\bar{c}_g$	mean geometric chord $\left(\frac{S}{b}\right)$, inches
c_r	wing root chord (in plane of symmetry), inches
c_t	wing tip chord, inches

C_D	total drag coefficient $\left(\frac{\text{drag}}{q_o S}\right)$
$C_{D_{min}}$	minimum total drag coefficient
ΔC_D	rise in total drag coefficient above minimum $\left(C_D - C_{D_{min}}\right)$
C_L	lift coefficient $\left(\frac{\text{lift}}{q_o S}\right)$
$C_{L_{opt}}$	lift coefficient for maximum lift-drag ratio
$\frac{dC_L}{d\alpha}$	lift-curve slope, per radian unless otherwise specified
ΔC_L	change in lift coefficient from value for minimum drag $\left(C_L - C_{L_{D\,=\,min}}\right)$
$\frac{\Delta C_D}{\left(\Delta C_L\right)^2}$	drag-rise factor
$(L/D)_{max}$	maximum lift-drag ratio
$C_{m_{\frac{1}{4}}}$	pitching-moment coefficient about 25 percent mean aerodynamic chord $\left(\frac{\text{pitching moment about 25 percent mean aerodynamic chord}}{q_o S \bar{c}}\right)$
C_N	normal-force coefficient $\left(\frac{\text{normal force}}{q_o S}\right)$

h	location of maximum airfoil thickness, measured from leading edge in streamwise direction, inches
m	ratio of the cotangent of the sweep angle of the leading edge to the cotangent of the sweep angle of the Mach line
M_n	Mach number corresponding to velocity component perpendicular to wing leading edge
q_o	free-stream dynamic pressure, pounds per square inch
R	Reynolds number based on mean geometric chord of wing
S	wing plan-form area including the area obtained by extending the wing leading and trailing edges to the fuselage center line, square inches
t	maximum thickness of airfoil section, inches
V_o	free-stream velocity, feet per second
X	distance from moment axis to center of lift, inches
Y	lateral coordinate, inches
y_c	maximum ordinate of mean camber line, inches
$\Lambda_{L.E.}$	sweep angle of leading edge, degrees

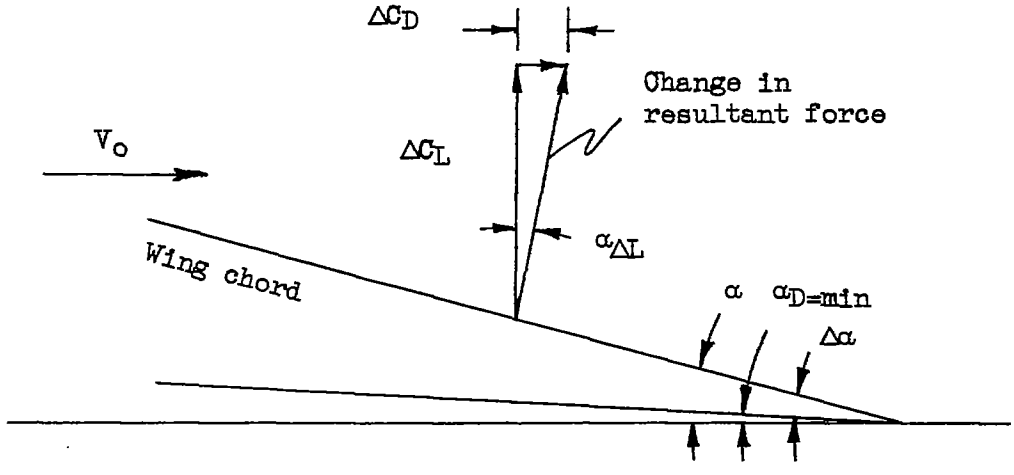

α	angle of attack, degrees
α_t	angle of twist, relative to wing root chord, degrees
$\Delta\alpha$	change in angle of attack from value for minimum drag, degrees
$\alpha_{\Delta L}$	rearward inclination of the change in resultant force corresponding to the change in lift coefficient ΔC_L, degrees
k_a	angle ratio $\left(\frac{\alpha_{\Delta L}}{\Delta\alpha}\right)$

Subscripts

D = min	value at minimum drag
L = 0	value at zero lift
opt	value at optimum lift coefficient

Model Configurations

Each wing-fuselage combination is designated by the letters WF followed by the number of degrees of leading-edge sweep. The letter c has been added after the sweep angle to differentiate the present configurations from those of the preceding investigation (reference 2).

DESCRIPTION OF APPARATUS

Wind Tunnel and Balance

The investigation was performed in the Ames 1- by 3-foot supersonic wind tunnel No. 1, which was fitted temporarily with a fixed nozzle designed to give a Mach number of 1.5 in a 1- by 2-1/2-foot test section. The tunnel, electric strain-gage balance, and instrumentation are described in references 5 and 6.

Models

A photograph of the model used in the investigation is shown in figure 1 and the design dimensions of the basic configuration (63° leading-edge sweep) are shown in figure 2. The fuselage and wing plan form are the same as those of the basic configuration in the tests of reference 2. (Because of the small model size and the method of assembling the wings and fuselage, the model dimensions vary slightly from those of reference 2 and figure 2. However, no significant alteration in plan form results from these small changes.) In the design of the present wing, three major parameters, the wing twist, the wing-section camber, and the wing-section thickness were changed from the values used for the original wing of reference 2. It is convenient to consider the changes in camber and twist together and then discuss the change in wing thickness.

The location of the sections for which mean camber lines and angles of twist were calculated are shown in figure 3. The ordinates of these sections, which are given in table I, were determined by the method discussed by Jones in reference 1. In that report it is shown that oblique vortices swept at angles corresponding to the leading and trailing edges can be used to determine the surface shape necessary to obtain a uniform lifting pressure distribution for a given lift coefficient and Mach number. The values of 0.25 and 1.53 were chosen as the design lift coefficient and Mach number, respectively. This value of lift coefficient was selected since it was believed that it would be close to that for maximum lift-drag ratio at a Mach number of 1.53. As was noted in reference 1, the calculated mean camber lines necessary to obtain a uniform lifting load for this type of wing plan form closely resemble the $a = 1.0$ mean camber line (see reference 7) used in subsonic airfoil design. For this reason the calculated mean camber line at each of the sections shown in figure 3, with the exception of that at the root, was approximated in the model design by $a = 1.0$ mean line which had the same maximum camber ordinate as was determined by theory.

As was also discussed in reference 1, the angle of attack of the section at the wing root theoretically must be 90° to maintain a uniform lifting pressure distribution over the entire wing at the design condition; that is, if the leading edge is assumed to be fixed in a horizontal plane parallel to the free-stream direction, the trailing edge of the wing would be directly below the leading edge at the root section. At the tip, the trailing edge would be above the plane in which the leading edge lies. However, since the sections near the root which theoretically require high values of α_t are

enclosed by the fuselage, the variation required by theory was not maintained in this region. Instead, the trailing-edge position at the root was obtained by assuming a nearly linear variation of twist inboard of the chord c_1. This deviation gave a value of 2.45° for the root-section angle of attack. To provide a convenient reference for angle-of-attack measurements, the wing was rotated to give 0° incidence at the root chord when referred to the longitudinal axis of the fuselage. The corresponding theoretical angle of attack at the tip was then -4.45° for the design load condition. Since, however, the bending of a swept-back wing under load contributes an increment of twist the calculated angles of twist were reduced as shown in figure 4. The procedure used to determine the twist with no load was to subtract from the calculated twist the amount expected from the wing deflection at the design lift coefficient for a tunnel pressure of 18 pounds per square inch absolute (q_o = 7.7 lb/sq in.). At the wing-tip section the calculated angle of twist due to bending was approximately -1.0° and this value agreed closely with that observed during tunnel operation. The angles of twist shown in figure 3 are those calculated for no aerodynamic load.

The thickness-chord ratio of the basic wing was reduced in the present investigation from that used with the 63° swept wing of reference 2. An NACA 64A005 thickness distribution in the stream direction was used in place of an NACA 64A006 section. This modification was suggested by a consideration of the flow conditions perpendicular to the wing leading edge. As was discussed in reference 2, the wing section perpendicular to the leading edge of the 63° swept wing was approximately 11 percent thick. At a free-stream Mach number of 1.53, corresponding to a Mach number normal to the leading edge of 0.69, it was considered probable that conditions associated with shock stall existed over the upper surface at lift coefficients below that for maximum lift-drag ratio. Therefore, some improvement might be realized by reducing the thickness-chord ratio of the wing section perpendicular to the leading edge to approximately 9 percent by using an NACA 64A005 thickness distribution in the stream direction. It was believed that both this reduction in thickness and the use of camber and twist would delay to a higher lift coefficient the conditions producing shock stall.

To investigate the characteristics of configurations with 67.0° and 70.0° of leading-edge sweep, each half of the 63° wing was rotated about the midpoint of the root chord. The changes in wing geometry resulting from changes in sweep are shown in table II. In each case the incidence of the wing root chord was set at 0° with reference to the longitudinal axis of the fuselage.

TEST METHODS

The methods used for obtaining the experimental force data are described in references 5 and 6. Measurements were made of lift, drag, and pitching moment through an angle-of-attack range of -2° to 8° at a Mach number of 1.53. The Reynolds number was varied within the range of 0.31 to 0.95 million based on the mean geometric chord. The liquid-film technique which was used to determine the nature of the boundary-layer flow and the corrections that were applied to the data are described in detail in reference 2. The precision of the experimental data is the same as that of reference 6 and is as follows:

Quantity	Uncertainty for $C_L = 0$	Uncertainty for $C_L = 0.4$
Lift coefficient	±0.002	±0.005
Drag coefficient	± .0004	± .0016
Pitching-moment coefficient	± .002	± .011
Angle of attack	± .11°	± .15°

RESULTS AND DISCUSSION

The present investigation is primarily concerned with the determination of the effects of camber and twist on the maximum lift-drag ratio and pitching-moment characteristics of a wing-fuselage combination at a Mach number of 1.53. The subsequent discussion, for the most part, consists of a comparison of the characteristics of the cambered, twisted wing configuration (WF-63c) studied in the present investigation with the characteristics observed in an earlier investigation (reference 2) with a symmetrical untwisted-wing configuration (WF-63) which had the same wing plan form. Since the maximum lift-drag ratio of each configuration depends upon the minimum drag coefficient, the lift coefficient for minimum drag, and the drag-rise factor, the data are discussed in terms of these parameters. The relationship between them is shown by the following equations:

[redacted]

$$\left(\frac{L}{D}\right)_{max} = \frac{1}{2\left[\Delta C_D/(\Delta C_L)^2\right]\left(C_{L_{opt}} - C_{L_{D=min}}\right)} \quad (1)$$

where

$$C_{L_{opt}} = \sqrt{\frac{C_{D_{min}}}{\Delta C_D/(\Delta C_L)^2} + \left(C_{L_{D=min}}\right)^2} \quad (2)$$

(When $C_{L_{D=min}}$ equals zero, as it does for a symmetrical wing, these equations reduce to equations (3) and (4) of reference 2.) Since the drag-rise factor is related to $dC_L/d\alpha$ and k_a as shown by the following equation,

$$\frac{\Delta C_D}{(\Delta C_L)^2} = \frac{k_a}{dC_L/d\alpha} \quad (3)$$

these parameters are also discussed. The comparison of the results of the force tests with WF-63c and WF-63 is limited to the data obtained at a Reynolds number of 0.84 million since similar effects were noted at the lower value investigated (0.62 million). The effects of Reynolds number and sweep observed with the cambered, twisted wing configurations and the differences between the experimental results and those calculated by the linear theory are considered only briefly because these trends were similar to those discussed in detail in reference 2.

Table III summarizes the experimental results obtained with the WF-63c, WF-67c, and WF-70c configurations at all Reynolds numbers investigated and includes, for purposes of comparison, the results presented in reference 2 with the WF-63 configuration at a Reynolds number of 0.84 million. Theoretical values of $dC_L/d\alpha$, $\Delta C_D/(\Delta C_L)^2$, and k_a are also included for the 63° and 67° swept wings. Since the linear theory indicates that these parameters are not affected by thickness, camber, or twist, they are the same as those listed

in reference 2 for identical plan forms. Theoretical values for the other aerodynamic parameters have not been determined because of the unknown effects of wing-fuselage interference.

Comparison of Lift, Drag, and Pitching-Moment Characteristics of WF-63c and WF-63

Lift-curve slope.- Figure 5 shows the experimental lift and pitching-moment characteristics of the WF-63c and WF-63 configurations. Also shown, for purposes of comparison, is the WF-63c lift curve which has been horizontally displaced to pass through the origin. The experimental value of $\alpha_{L=0}$ of 1.2° for WF-63c is associated with the selection of the wing root chord as the angle-of-attack reference. As was discussed previously, this chord was arbitrarily set at zero incidence to the longitudinal axis of the fuselage. It was observed in the tests of reference 8 that a positively cambered, untwisted wing swept within the Mach cone had positive lift at zero angle of attack. However, the wing twist of WF-63c, is sufficient to cause a larger increment of negative lift at zero angle of attack of the root chord than is obtained as positive lift through the use of camber.

A comparison of the WF-63c displaced lift curve with that for WF-63 shows that, although the slope near zero lift was greater for the cambered, twisted wing configuration, there was no appreciable change in slope above $C_L = 0.10$. The difference near zero lift between the two configurations makes the average slope slightly higher for WF-63c, and this change has some bearing on the subsequent discussion of the drag rise.

Drag.- Figure 6 presents the drag curves obtained with WF-63c and WF-63. An additional drag curve is also shown, which has been obtained by displacing vertically the curve for WF-63c by the difference in minimum drag coefficient obtained experimentally between the two configurations. This curve separates the effects of the change in minimum drag coefficient from the changes in the lift coefficient for minimum drag and rate of drag rise with lift coefficient.

As shown in table III, at a Reynolds number of 0.84 million the measured values of minimum drag coefficient indicate a decrease from 0.0160 for WF-63 to 0.0140 for WF-63c. This change appears to be primarily a result of the reduction in wing thickness from 6 to 5 percent. As was noted in reference 2, the theoretical wing-thickness pressure drag of the wing of WF-63 is approximately 0.0047. Since the linear theory indicates that this component of the minimum drag

coefficient varies as $(t/c)^2$, a large part (approximately 0.0014) of the experimentally observed minimum drag-coefficient change can be attributed to the reduction in wing thickness. The remaining difference is probably associated with a reduction in the skin friction, the separation pressure drag for the WF-63c configuration, or with the experimental uncertainty.

A comparison of the displaced WF-63c drag curve with that for WF-63 (fig. 6) shows that, at lift coefficients near that for maximum lift-drag ratio, ΔC_D is considerably less for WF-63c than for WF-63. This reduction can be attributed to the displacement of the minimum of the drag curve to a positive lift coefficient and a decrease in the rate of rise of the drag curve. The increase in $C_{L_{D = min}}$ is caused by the camber and twist and is similar to that obtained at subsonic speeds. The decrease in drag-rise factor (equation (3)) is associated with a reduction in the rearward inclination of the change in the resultant force vector, as indicated by the values of k_a in table III, and also with the previously mentioned slight increase in the average lift-curve slope.

Liquid-film tests were made with both configurations at a lift coefficient of 0.21 to determine any change in boundary-layer flow associated with the observed reduction in k_a. These tests were made at a slightly lower Reynolds number (0.62 million) where a similar reduction in k_a was noted. The results are presented in figure 7 which shows that laminar separation occurred on the upper surface of both wings, but with the wing of WF-63c the total area of separated flow, particularly near the leading edge, was reduced. This reduction in leading-edge separation would be expected to reduce the magnitude of k_a since it is probably accompanied by a smaller loss in leading-edge suction force. It should be noted particularly that the wing camber and twist were effective in reducing leading-edge separation on the outboard wing sections.

Another factor which is probably associated with the reduction of ΔC_D at lift coefficients below the optimum for WF-63c is the reduction in wing thickness and its effect in delaying to a higher lift coefficient the occurrence of shock stall. However, the lack of experimental pressure-distribution measurements for both wings prevents an evaluation of the magnitude of this effect which, in the analysis of the force-test results, cannot be isolated from similar effects expected of camber and twist.

Maximum lift–drag ratio.– Figure 6 shows the lift–drag curves obtained with the two configurations discussed in the preceding sections. It also shows an additional lift–drag curve which can be used to separate the effects of the change in minimum drag coefficient from that due to changes in the lift coefficient for minimum drag and rate of drag rise. This lift–drag curve has been determined from the WF–63c drag curve that was displaced as previously discussed. The experimental data show that an increase in maximum lift–drag ratio from 7.2 and 8.3 resulted from the use of the cambered, twisted, thinner wing. The supplementary curve indicates that this improvement results to an approximately equal degree from the reduction in minimum drag coefficient and from the combined effect of the displacement of the minimum of the drag curve to a positive lift coefficient and the reduction in drag rise previously discussed.

Pitching moment.– The effect of the camber and twist on the variation of pitching–moment coefficient with lift coefficient can be seen in figure 5, where the moment coefficients have been computed with the moment reference axis at 25 percent of the mean aerodynamic chord. Also included are the approximate variations of the center of lift for the two configurations. These variations were determined from the moment data by the following equation:

$$\frac{X}{c} = \frac{C_{m_{\frac{1}{4}}} - \left(C_{m_{\frac{1}{4}}}\right)_{L=0}}{C_N} \qquad (4)$$

The term $\left(C_{m_{\frac{1}{4}}}\right)_{L=0}$ has been included in this equation so that the resulting values of $\frac{X}{c}$ are equal (in percent of the mean aerodynamic chord) to the distances from the moment axis to the center of the lift. If the term $\left(C_{m_{\frac{1}{4}}}\right)_{L=0}$ is omitted, the value of $\frac{X}{c}$ gives the position of the center of pressure with a value of infinity being obtained at zero lift. It should be noted that equation (4) gives the aerodynamic–center location when the right–hand side is a

constant throughout the lift-coefficient range; that is, in cases where the moment curve is linear, the center-of-lift position remains fixed throughout the lift-coefficient range.

Considering both the positive and negative ranges of lift coefficient, figure 5 shows that WF-63c at this Reynolds number has a slightly greater total center-of-lift travel. However, in the positive range of lift coefficients near $C_{L_{opt}}$ there is a favorable reduction in the rate of change of center-of-lift position with lift coefficient for WF-63c. The relatively large changes in center-of-lift location near zero lift with both configurations are believed to be due to the effects of laminar boundary-layer separation. As will be discussed later, these changes may be expected to decrease at higher Reynolds numbers.

Effects of Sweep

Figures 8, 9, and 10 present the experimental data for the cambered, twisted wing configurations with leading-edge sweep angles of 63.0°, 67.0°, and 70.0°. The values of the aerodynamic parameters determined from these data are listed in table III for all Reynolds numbers investigated.

The decrease in lift-curve slope with increased sweep observed with these configurations (fig. 8) is similar to that obtained in reference 2 with the symmetric wing configurations, where it was noted that this trend is indicated by the linear theory. The variations of minimum drag coefficient and drag-rise factor (fig. 9) are also similar to those noted in the earlier investigation. The decrease in minimum drag coefficient is caused by a decrease in wing-thickness pressure drag with increased sweep. The increase in drag-rise factor with increased sweep is primarily associated with the decrease in lift-curve slope. As a result of these two opposing variations of drag with sweep, there is an optimum leading-edge sweep angle for maximum lift-drag ratio. As in reference 2, the optimum angle in the present investigation was found to be near 67° for this type of configuration at a Mach number of 1.53.

Separation of the laminar boundary layer at the low test Reynolds numbers caused relatively large changes in center-of-lift location with changes in lift coefficient for all configurations. These changes are shown in figure 10. The effects of separation are most pronounced at low lift coefficients for all configurations, as is indicated by the large change in center-of-lift position with lift coefficient near

zero lift. Parts (a), (b), and (c) of figure 10 show the effect of sweep on the pitching-moment characteristics of the three configurations for a Reynolds number of 0.62 million.

Effects of Reynolds Number

Since the present series of tests were performed at low Reynolds numbers, the results are not directly applicable to full-scale design studies because the effects of Reynolds number are apparently large. However, the data do permit some predictions to be made of the trends at higher Reynolds numbers. Equations (1) and (2) show that the maximum lift-drag ratio of each configuration depends upon the values of minimum drag coefficient, drag-rise factor, and lift coefficient for minimum drag. An examination of the values listed in table III shows that increasing the Reynolds number with the WF-63c and WF-67c models produced favorable changes of all of these parameters.

The reduction in $C_{D_{min}}$ with increased Reynolds number is similar to that discussed in reference 2, where it was observed that a decrease in the area of separated flow caused a decrease in the separation drag at zero lift. This favorable effect should continue with increased Reynolds number, since transition of the laminar boundary layer to turbulent flow may be expected on the basis of the liquid-film test results of reference 9.

The reduction in the magnitude of the drag-rise factor observed in the present investigation would also be expected to continue with increased Reynolds number, particularly if turbulent flow were obtained over the forward part of the wing. With turbulent boundary-layer flow, the separated area observed on the outboard upper surface near the trailing edge of the lifting wing (fig. 7) would be expected to decrease and hence to reduce the pressure drag. The experimental wing pressure drag is also associated with the extent of the separation bubble near the inboard leading edge of the upper surface. Subsonic tests (reference 10) have shown that the chordwise extent of this separated area is reduced with increased Reynolds number, since reattachment of the turbulent boundary layer occurs farther forward on the wing. This reduction in separation is accompanied by a decrease in the pressure over the wing leading edge which, particularly when realized with a rounded leading-edge airfoil section, will also result in a decrease in pressure drag. Although no significant change in lift-curve slope was observed in the present tests as a result of increasing the Reynolds number, it is probable that a decrease in the area of separated flow near the trailing edge will result in some improvement of this characteristic and consequently, as shown by equation (3),

would cause a further decrease in the drag-rise factor.

Increasing the Reynolds number with WF-63c and WF-67c increased the value of $C_{L_{D=min}}$ as is shown in table III. This fact suggests further increases at higher Reynolds numbers. However, because of the unknown effects of camber, twist, and separation at these low Reynolds numbers, it is difficult to estimate the change to be expected at full-scale Reynolds numbers.

The effect of increased Reynolds number on the values of maximum lift-drag ratio of the WF-63c and WF-67c configurations is shown in figures 9(a) and (b). With WF-63c, values of $(L/D)_{max}$ of 7.3 and 8.3 were obtained at Reynolds numbers of 0.62 and 0.84 million, respectively. With the WF-67c configuration, values of 6.6, 7.7, and 9.0 were obtained at Reynolds numbers of 0.31, 0.62, and 0.95 million, respectively. It appears, therefore, that increases in Reynolds number beyond the range of the present investigation will probably be accompanied by further increases in maximum lift-drag ratio.

In view of the expected change in boundary-layer flow at higher Reynolds numbers, the pitching-moment characteristics of the small-scale configurations, which had large areas of separated flow at all lift coefficients, are of questionable quantitative value. It may be expected that if the laminar separation areas are eliminated, or considerably reduced near zero lift at higher Reynolds numbers, the relatively large change in center-of-lift position in this range (fig. 10) will also be reduced. This possible improvement is indicated when the center-of-lift curves of figures 10(d) and (e) are compared with those of figures 10(a) and (b). At the higher Reynolds numbers, with the WF-63c and WF-67c configurations, the rearward shift of the center of lift near a lift coefficient of 0.10 is also reduced. This shift occurs when the boundary layer separates near the wing leading edge because the separation results in a decrease in the negative pressures on the forward part of the upper surface of the inboard sections. Consequently, the reduction in this rearward shift with increased Reynolds number is attributed to a decrease in the chordwise extent of the leading-edge separation bubble because such a change would cause a smaller decrease in the negative pressure peak near the wing leading edge.

CONCLUDING REMARKS

The results of tests made at a Mach number of 1.53 with a wing-fuselage combination employing a cambered and twisted wing with 63°

leading-edge sweep when compared with results obtained with a similar configuration using a thicker wing with no camber or twist have shown an increase in maximum lift-drag ratio from 7.2 to 8.3 at a Reynolds number of 0.84 million. This increase resulted from a decrease in minimum drag coefficient, a displacement of the minimum of the drag curve to a positive lift coefficient, and a slight decrease in the rate of drag rise. The total center-of-lift travel with the cambered-twisted-wing configuration was slightly greater than that with the symmetrical wing, but the change in center-of-lift location with lift coefficient was reduced at values near that for maximum lift-drag ratio.

Additional tests conducted with configurations having cambered and twisted wings with 67° and 70° leading-edge sweep at a Reynolds number of 0.62 million indicated the leading-edge sweep angle for maximum lift-drag ratio at a Mach number of 1.53 was approximately 67°. These tests also showed that, with increased sweep, the lift-curve slope and minimum drag coefficient was decreased and the rate of drag rise with lift coefficient was increased.

Tests made with the configurations employing wings with leading-edge sweep angles of 63° and 67° to study the effects of Reynolds number showed that with increased Reynolds number the value of maximum lift-drag ratio was increased. At 63° sweep, values of 7.3 and 8.3 were obtained at Reynolds numbers of 0.62 and 0.84 million, respectively; and at 67° sweep, values of 6.6, 7.7, and 9.0 were obtained at Reynolds numbers of 0.31, 0.62, and 0.95 million, respectively. These results indicate that further improvement at full-scale Reynolds numbers may be expected. Increasing the Reynolds number with the 63° configuration also produced a favorable reduction in total center-of-lift travel with lift coefficient

Ames Aeronautical Laboratory,
National Advisory Committee for Aeronautics,
Moffett Field, Calif.

[redacted]

REFERENCES

1. Jones, Robert T.: Estimated Lift-Drag Ratios at Supersonic Speed. NACA TN No. 1350, 1947.

2. Madden, Robert T.: Aerodynamic Study of a Wing-Fuselage Combination Employing a Wing Swept Back 63°.- Characteristics at a Mach Number of 1.53 Including Effect of Small Variations of Sweep. NACA RM No. A8J04, 1949.

3. McCormack, Gerald M., and Walling, Walter C.: Aerodynamic Study of a Wing-Fuselage Combination Employing a Wing Swept Back 63°.- Investigation of a Large-Scale Model at Low Speed. NACA RM No. A8D02, 1949.

4. Reynolds, Robert M., and Smith, Donald W.: Aerodynamic Study of a Wing-Fuselage Combination Employing a Wing Swept Back 63°.- Subsonic Mach and Reynolds Number Effects on the Characteristics of the Wing and on the Effectiveness of an Elevon. NACA RM No. A8D20, 1948.

5. Van Dyke, Milton D.: Aerodynamic Characteristics Including Scale Effects of Several Wings and Bodies Alone and in Combination at a Mach Number of 1.53. NACA RM No. A6K22, 1947.

6. Vincenti, Walter G., Nielsen, Jack, N., and Matteson, Frederick H.: Investigation of Wing Characteristics at a Mach Number of 1.53.- I - Triangular Wings of Aspect Ratio 2. NACA RM No. A7I10, 1947.

7. Abbott, Ira H., von Doenhoff, Albert E., and Stivers, Louis S., Jr.: Summary of Airfoil Data. NACA ACR No. L5C05, 1945.

8. Vincenti, Walter G., Van Dyke, Milton D., and Matteson, Frederick H.: Investigation of Wing Characteristics at a Mach Number of 1.53. II - Swept Wings of Taper Ratio 0.5. NACA RM No. A8E05, 1948.

9. Frick, Charles W., and Boyd, John W.: Investigation at Supersonic Speed (M = 1.53) of the Pressure Distribution Over a 63° Swept Airfoil of Biconvex Section at Zero Lift. NACA RM No. A8C22, 1948.

10. von Doenhoff, Albert E., and Tetervin, Neal: Investigation of the Variation of Lift Coefficient with Reynolds Number at a Moderate Angle of Attack on a Low-Drag Airfoil. NACA CB, Nov. 1942.

TABLE I.— TABLE OF ORDINATES FOR AIRFOIL SECTIONS SHOWN IN FIGURE 3

c_0		c_1				c_2			
$x_{U,L}$	$y_{U,L}$	x_U	y_U	x_L	y_L	x_U	y_U	x_L	y_L
0	0	0	0	0	0	0	0	0	0
.5	.404	.474	.438	.526	−.366	.469	.457	.532	−.357
.75	.488	.726	.536	.778	−.433	.713	.557	.788	−.419
1.25	.616	1.221	.690	1.283	−.536	1.208	.720	1.295	−.507
2.50	.847	2.463	.984	2.535	−.706	2.447	1.026	2.547	−.663
5.00	1.166	4.956	1.401	5.039	−.927	4.944	1.477	5.056	−.851
10.0	1.599	9.959	1.984	10.041	−1.211	9.944	2.103	10.056	−1.089
20.0	2.131	19.964	2.725	20.036	−1.530	19.956	2.912	20.044	−1.345
30.0	2.413	29.974	3.138	30.026	−1.685	29.969	3.373	30.031	−1.458
40.0	2.499	39.990	3.297	40.010	−1.700	39.987	3.548	40.013	−1.446
50.0	2.354	50.000	3.179	50.00	−1.530	50.000	3.436	50.000	−1.270
60.0	2.032	60.010	2.828	59.990	−1.231	60.013	3.085	59.987	−.982
70.0	1.589	70.015	2.313	69.985	−.860	70.019	2.547	69.981	−.632
80.0	1.071	80.015	1.669	79.985	−.479	80.025	1.852	79.975	−.288
90.0	.541	90.015	.927	89.985	−.155	90.019	1.045	89.981	−.031
100.0	.011	100.000	— — —	100.000	— — —	100.000	— — —	100.000	— — —

Note: All values are given in percent chord.
For all sections: Leading-edge radius = 0.175. Trailing-edge radius = 0.014.

TABLE I.- Concluded

c_3			
x_U	y_U	x_L	y_L
0.470	0.462	0.533	-0.350
.709	.557	.788	-.414
1.202	.725	1.298	-.502
2.444	1.043	2.556	-.645
4.944	1.497	5.056	-.828
9.944	2.150	10.056	-1.051
19.952	2.978	20.048	-1.290
29.968	3.447	30.032	-1.377
39.984	3.639	40.016	-1.361
50.000	3.527	50.000	-1.186
60.016	3.169	59.984	-.892
70.024	2.627	69.976	-.557
80.024	1.911	79.976	-.223
90.016	1.091	89.984	.008
100.000	- - -	100.000	- - -

c_4			
x_U	y_U	x_L	y_L
0.470	0.460	0.536	-0.350
.711	.558	.799	-.405
1.204	.722	1.291	-.503
2.440	1.039	2.549	-.646
4.945	1.489	5.055	-.832
9.945	2.144	10.055	-1.050
19.956	2.976	20.044	-1.291
29.967	3.425	30.033	-1.389
39.978	3.621	40.022	-1.368
50.000	3.512	50.000	-1.193
60.011	3.162	59.989	-.908
70.022	2.604	69.978	-.569
80.022	1.915	79.978	-.230
90.022	1.083	89.978	.011
100.000	- - -	100.000	- - -

c_5			
x_U	y_U	x_L	y_L
0.473	0.455	0.543	-0.350
.718	.560	.788	-.420
1.208	.718	1.278	-.508
2.452	1.033	2.557	-.648
4.956	1.494	5.061	-.823
9.965	2.119	10.070	-1.068
19.947	2.960	20.053	-1.313
29.965	3.415	30.035	-1.419
39.982	2.608	40.018	-1.401
50.000	3.485	50.000	-1.208
60.018	3.135	59.982	-.928
70.018	2.592	69.982	-.595
80.018	1.891	79.982	-.245
90.018	1.068	89.982	-.018
100.000	- - -	100.000	- - -

Note: All values are given in percent chord.
For all sections: Leading-edge radius = 0.175. Trailing-edge radius = 0.014.

NACA

TABLE II.- SUMMARY OF GEOMETRIC PROPERTIES OF WINGS

Configuration	$\Lambda_{L.E.}$ (deg)	A	S (sq in.)	$\frac{c_t}{c_r}$	$\bar{c}$ (in.)	$\bar{c}_g$ (in.)	$\frac{t}{c}$	$\frac{h}{c}$	M_n	m
WF-63c	63.0	3.46	7.311	0.25	1.630	1.453	0.0500	40.0	0.69	0.59
WF-67c	67.0	2.75	7.270	.25	1.833	1.626	.0443	41.5	.60	.49
WF-70c	70.0	2.22	7.516	.25	2.078	1.841	.0396	42.6	.52	.42

Note: The aspect ratios and mean geometric chords are based on the wing area including that blanketed by the fuselage. The taper ratios and mean geometric chords neglect the slight rounding of the wing tips by assuming them to be straight lines parallel to the stream direction and tangent to the outermost actual tip contours.

TABLE III.- SUMMARY OF RESULTS

Configuration	R (million)	Lift			Drag				Lift-drag ratio	
		$\left(\frac{dC_L}{d\alpha}\right)_{L=0}$ (per deg)	$\left(\frac{dC_L}{d\alpha}\right)_{opt}$ (per deg)	$\alpha_{L=0}$ (deg)	$C_{D_{min}}$	$C_{L_{D=min}}$	$\left[\frac{\Delta C_D}{(\Delta C_L)^2}\right]_{opt}$	$k_{a_{opt}}$	$\left(\frac{L}{D}\right)_{max}$	$C_{L_{opt}}$
WF-63c	0.62	0.043 (.051)	0.045 (.051)	1.2	0.0155	0.005	0.314 (.185)	0.78 (.54)	7.3	0.24
	.84	.043 (.051)	.045 (.051)	1.2	.0140	.010	.289 (.185)	.71 (.54)	8.3	.23
WF-67c	.31	.038 (.043)	.043 (.043)	1.2	.0133	.000	.436 (.196)	.99 (.48)	6.6	.19
	.62	.038 (.043)	.043 (.043)	1.2	.0123	.010	.391 (.196)	.89 (.48)	7.7	.19
	.95	.038 (.043)	.043 (.043)	1.2	.0116	.015	.313 (.196)	.71 (.48)	9.0	.20
WF-70c	.62	.032	.034	1.0	.0111	.000	.440	.86	7.1	.16
Results from reference 2										
WF-63	.84	.038 (.051)	.045 (.051)	0.0 (.0)	.0160	0.0 (.0)	.300 (.185)	.74 (.54)	7.2	.21

Note: Where theoretical values have been determined they are indicated in parenthesis directly below the experimental result.

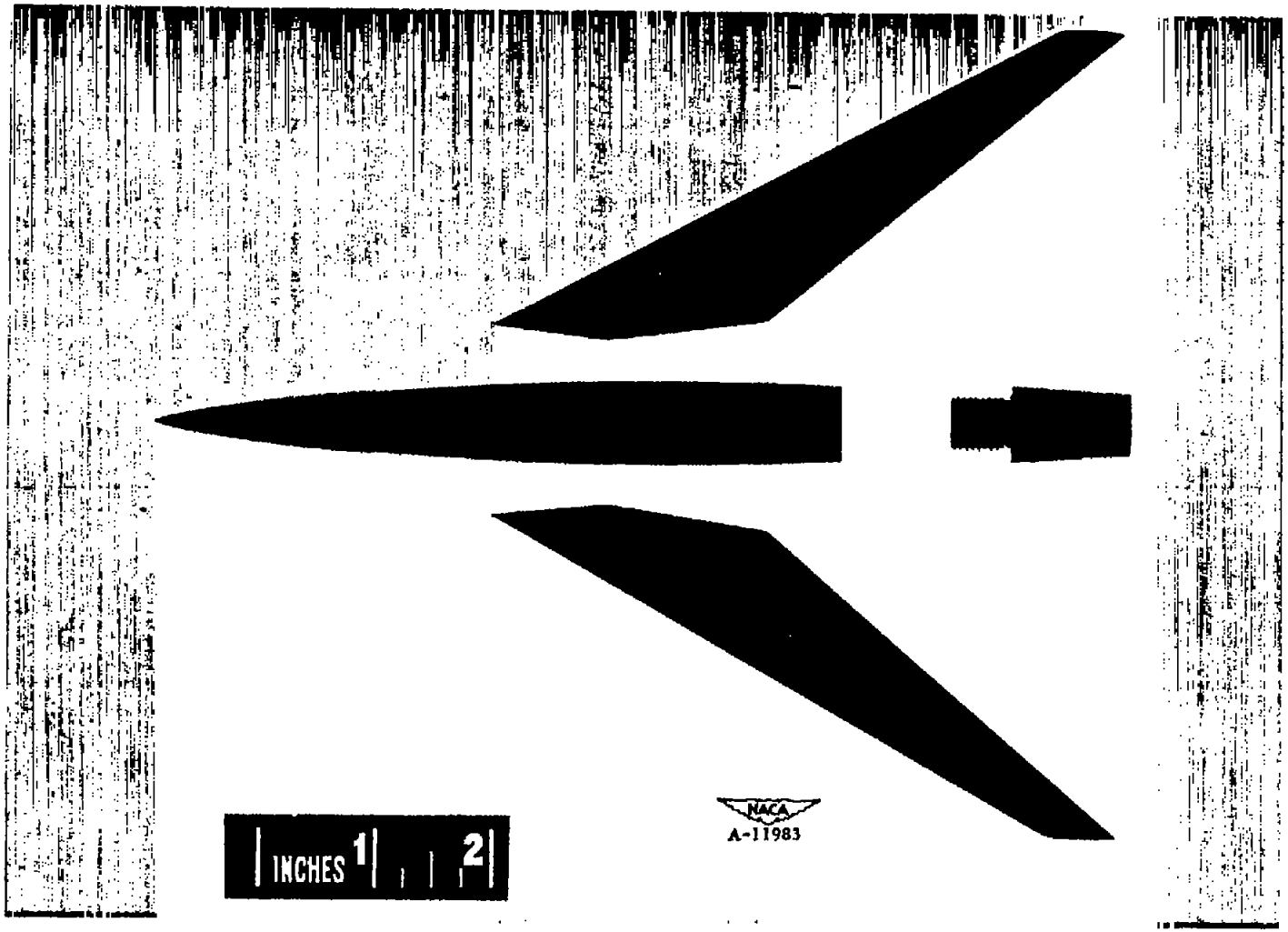

Figure 1.– Exploded view of Model.

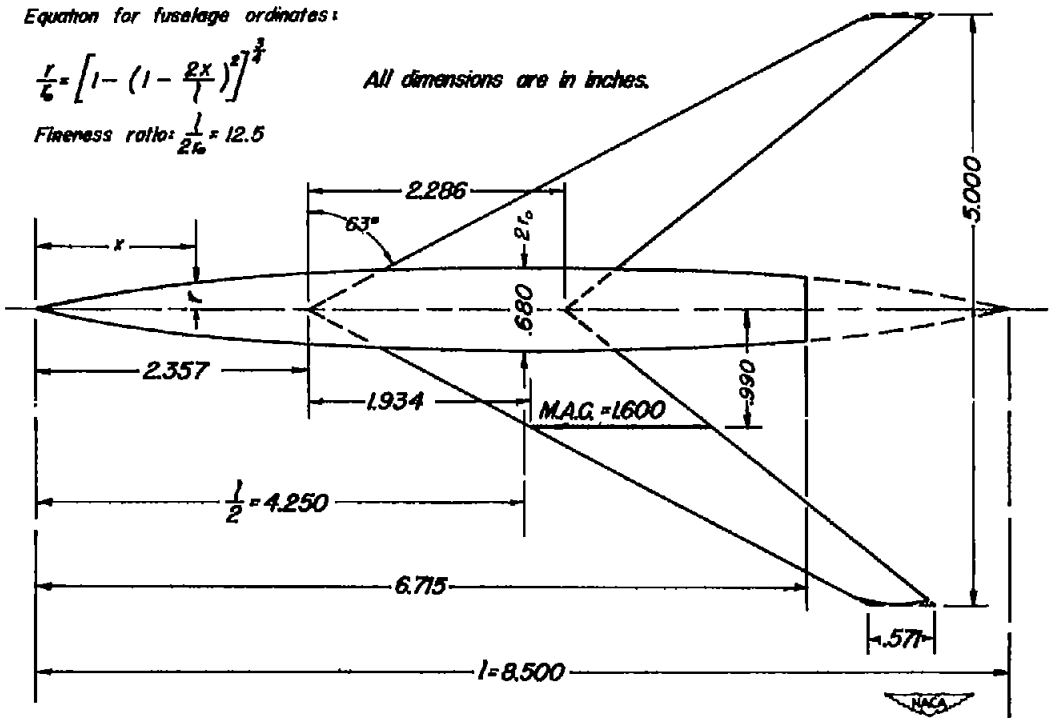

Figure 2.- Design dimensions of basic configuration, WF-63c.

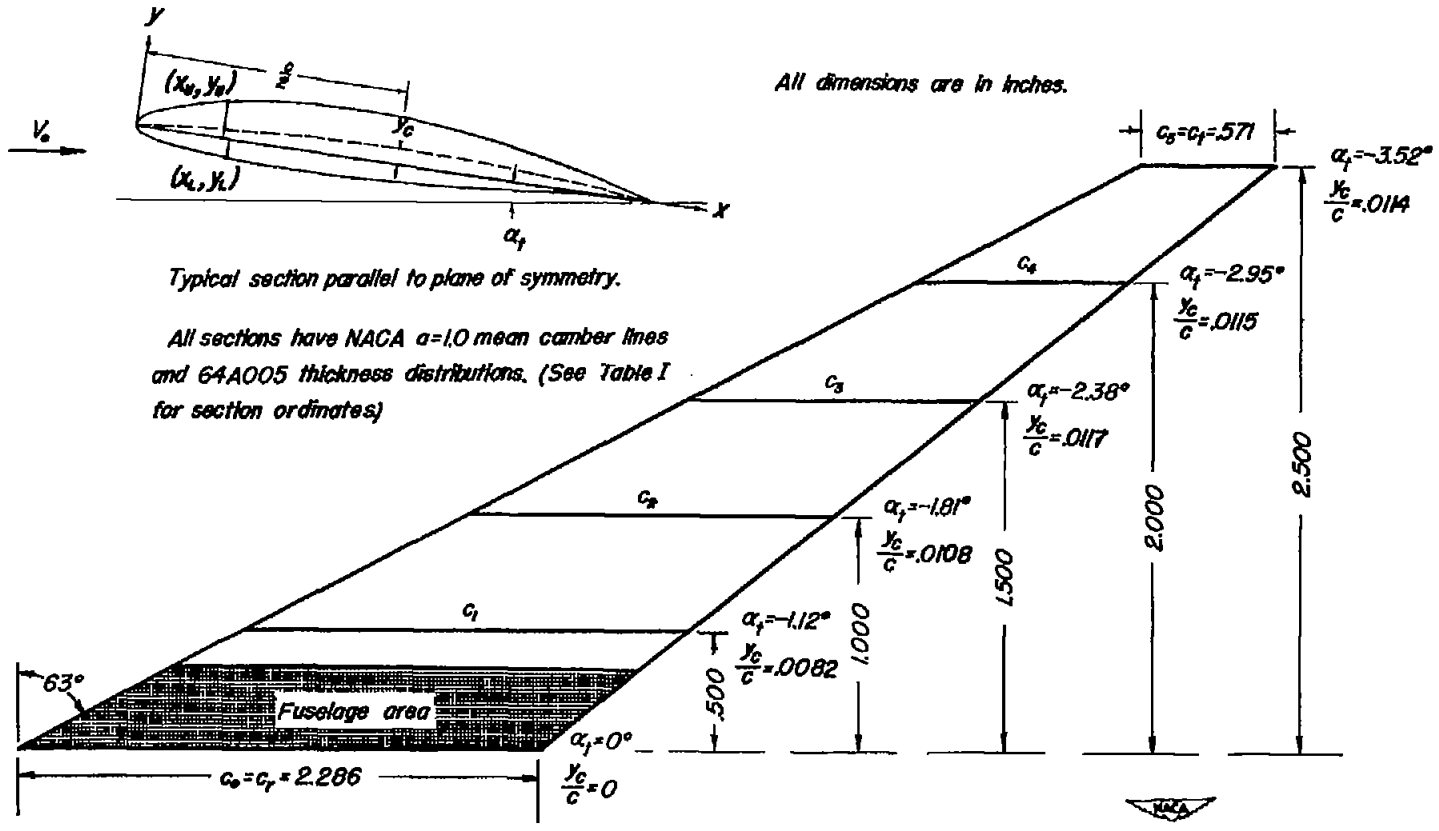

Figure 3.- Plan form of right half-wing showing location of sections for which camber ordinates and angles of twist were calculated.

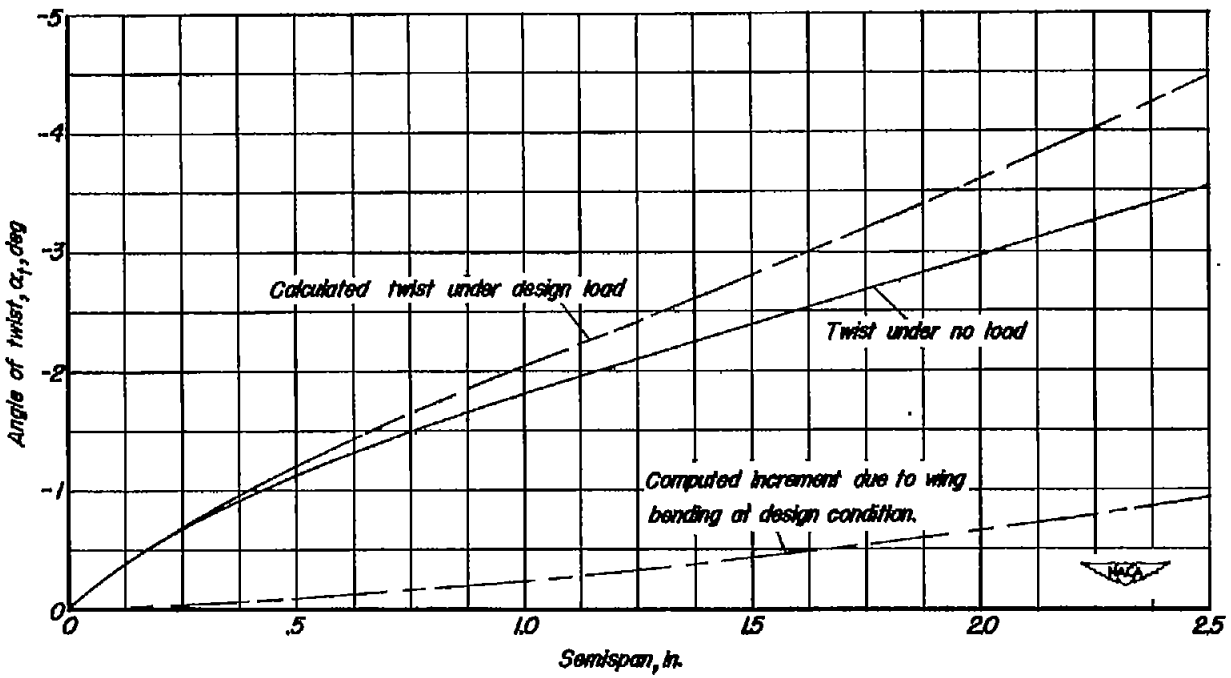

Figure 4.- Spanwise variation of wing twist.

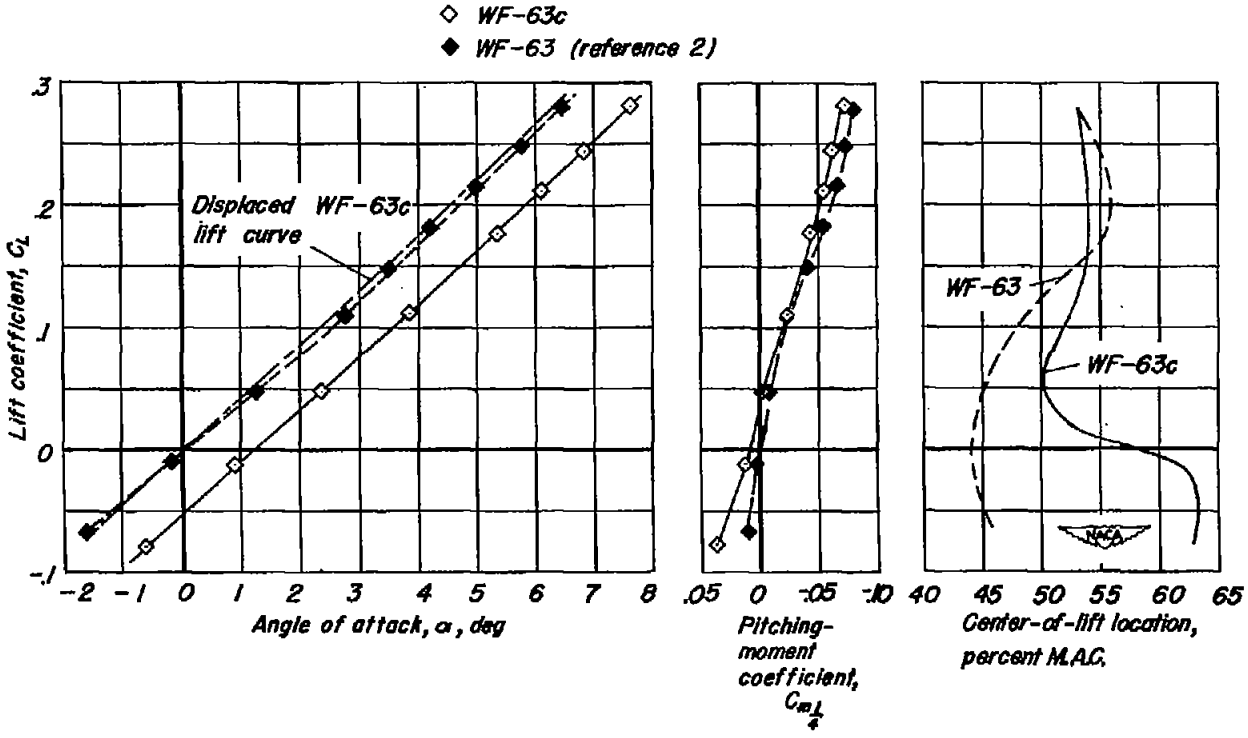

Figure 5.-Lift and pitching-moment characteristics of WF-63c and WF-63 at a Reynolds number of 0.84 million.

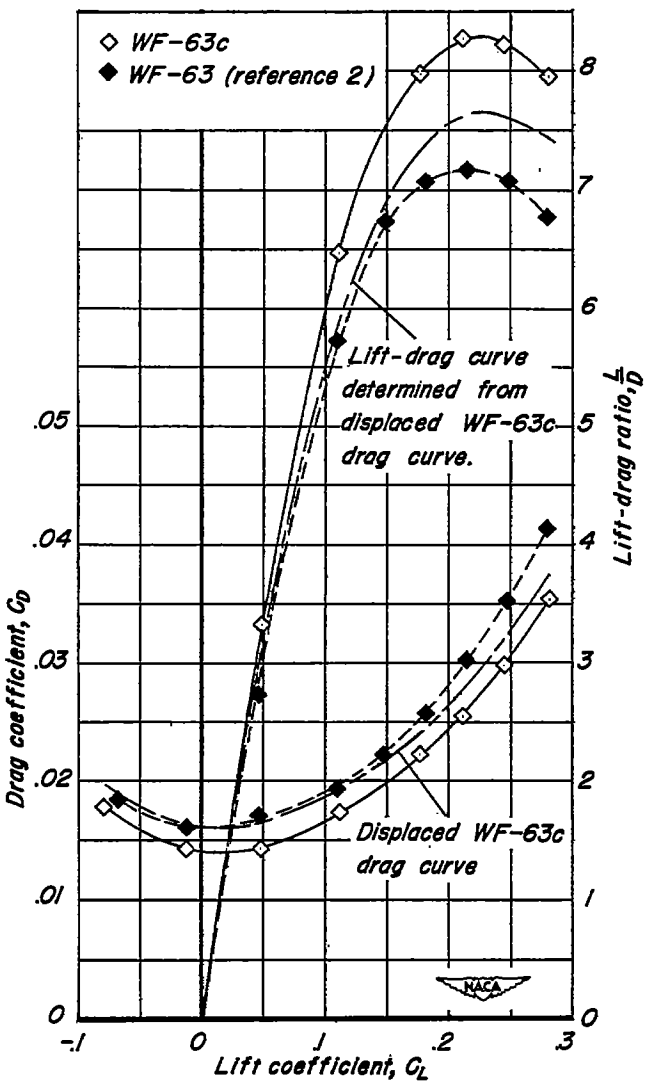

Figure 6.—Drag and lift-drag ratio characteristics of WF-63c and WF-63 at a Reynolds number of 0.84 million.

[redacted]

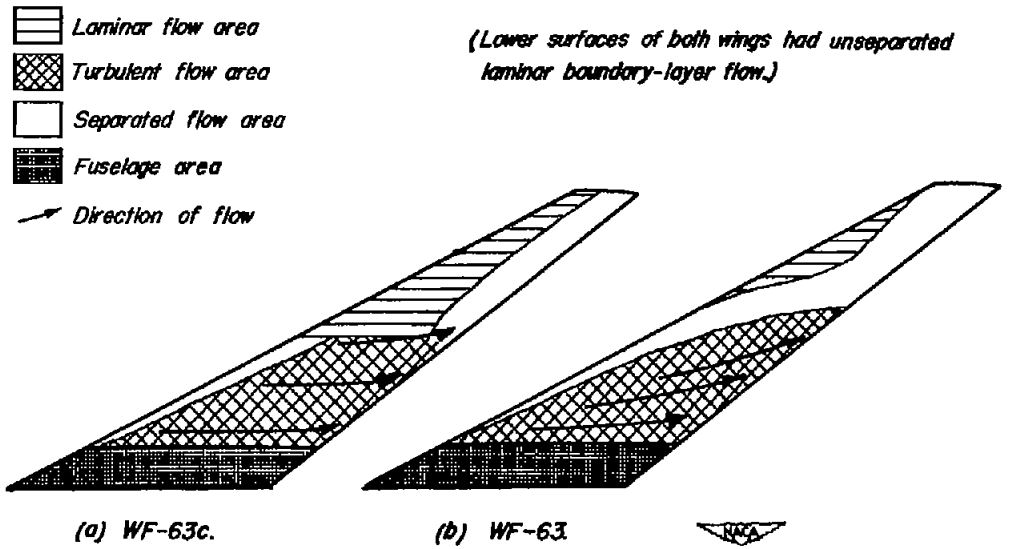

Figure 7.- Boundary-layer flow patterns on upper surfaces of WF-63c and WF-63 at a lift coefficient of 0.21 and Reynolds number of 0.62 million.

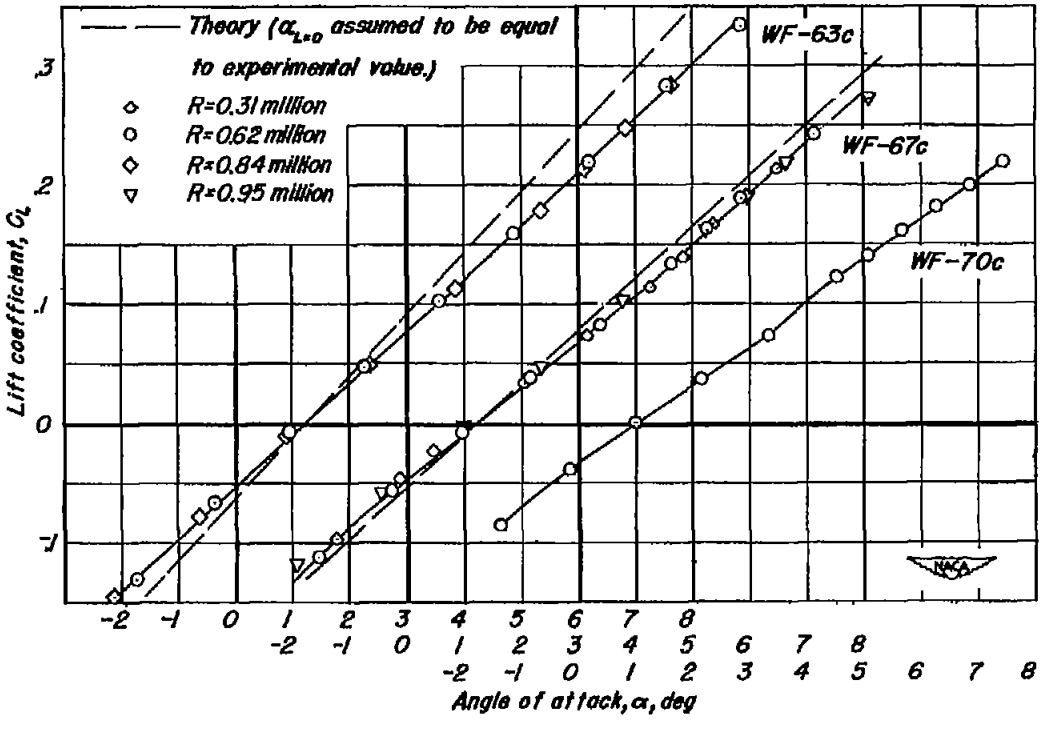

Figure 8.- Effects of sweep and Reynolds number on lift-curve slope.

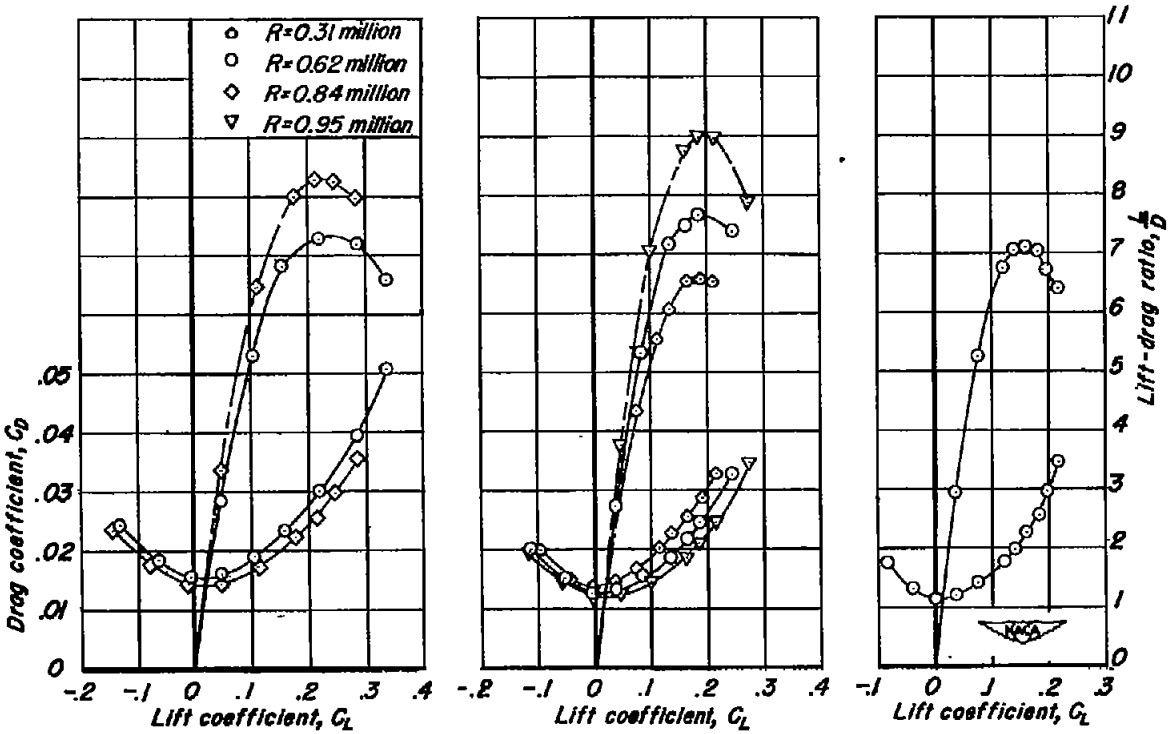

(a) WF-63c. (b) WF-67c. (c) WF-70c.

Figure 9.—Effects of sweep and Reynolds number on drag and lift-drag ratio.

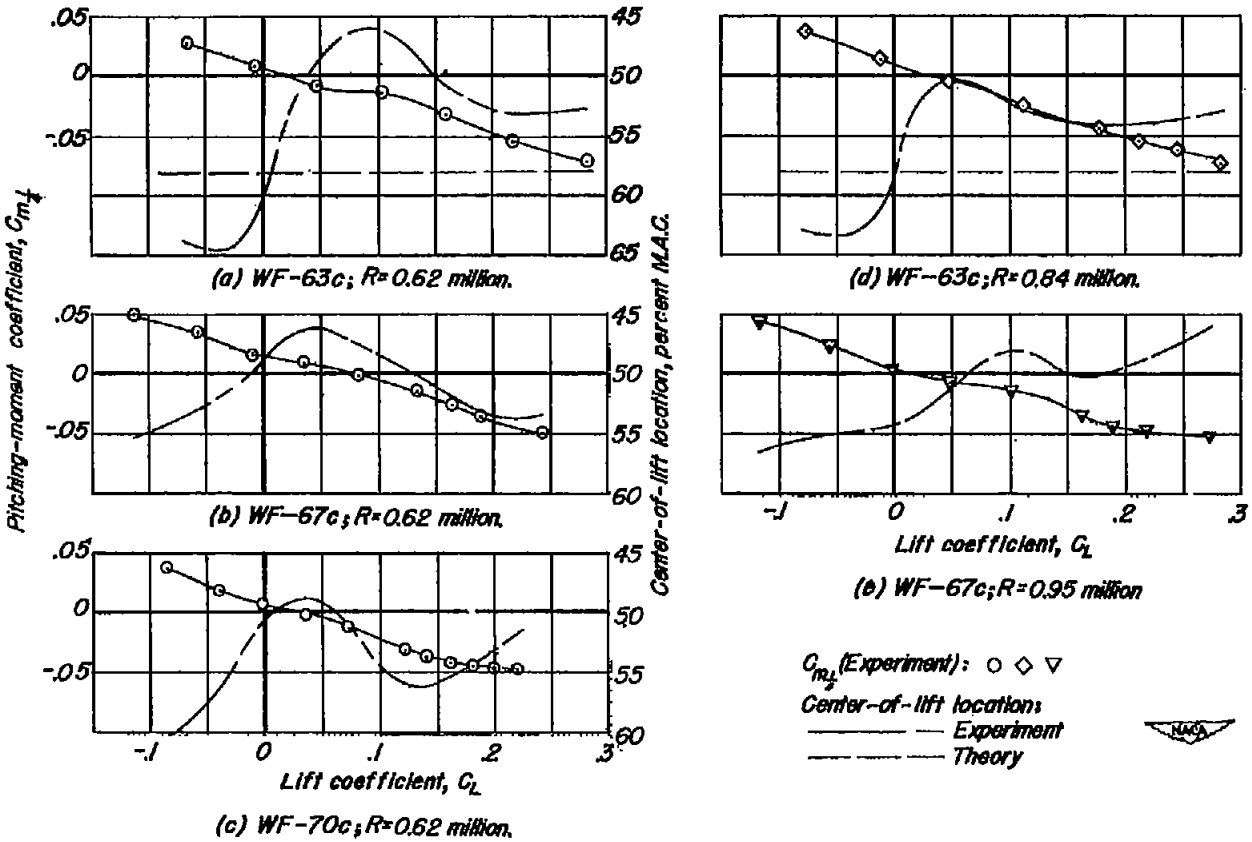

Figure 10.- Effects of sweep and Reynolds number on pitching moment.